Supplementary Materials

David Reens,* Hao Wu,* Tim Langen,† and Jun Ye
JILA, National Institute of Standards and Technology and the University of Colorado and Department of Physics, University of Colorado, Boulder, Colorado 80309-0440, USA
(Dated: October 4, 2017)

The present study on the role of mixed fields for spin-flip loss evolved out of our continuing investigations into the collisional processes of trapped OH molecules in a magnetic quadrupole trap reported in Refs. [1, 2]. The current investigations have revealed that the spin-flip loss can be substantially enhanced when an electric field is applied to the magnetic trap, and thus an important fraction of the inelastic collisional loss under various electric fields is in fact attributable to spin-flip losses. In Sections A, B we provide further information on the electric field-induced trap loss and evaporative cooling, respectively. In Section C we provide an algebraic derivation of the loss enhancement factor presented in Eqn. 3 of the main text [3].

A. Electric Field-Induced Trap Losses

Ref. [1] introduced the single particle spin-flip loss enhancement process and deconvoluted its effect from the inelastic collisional effect (Appendix A, Ref. [1]). Since that time, new and more systematic experimental observations have prompted improvements to the analysis that was presented there.

Relative to the previous approach, we make the same simplifying assumptions: loss only occurs in the $\vec{E} \perp \vec{B}$ plane, and only the velocity orthogonal to this plane matters as molecules cross this loss plane, and the in-trap population follows a thermalized Maxwell-Boltzmann distribution. Our improvement relates to the next step, where an integral calculation for the loss rate is performed. In Ref. [1] the integration spans the entire 3D spatial distribution, weighted by the frequency of crossing of the center plane and the chance of loss for each crossing:

$$\Gamma_{\mathrm{LZ}} = \int_0^\infty 4\pi r^2\, n(r) dr \int_0^\infty n(v_\theta) dv_\theta \left(\frac{v_\theta}{\pi r} P_{\mathrm{hop}}(r, v_\theta)\right). \quad (1)$$

Here $n(r)$ is the radial distribution function, constrained to satisfy $\int_0^\infty 4\pi r^2 n(r) = 1$, and of the form $n(r) \propto e^{-\mu_B B' r/kT}$. Likewise $n(v_\theta)$ is the usual normalized Maxwellian velocity distribution. Implicit in this integration is the assumption that molecules at a given radius r cross the center plane with a frequency of $v_\theta/\pi r$. This approximation is rather simplistic given that molecules are typically not following circular orbits of constant v_θ but are in general following some complex trap motion. A more accurate treatment which we use here is to perform an integration of flux through the loss plane directly:

$$\Gamma_{\mathrm{LZ}} = \int_0^\infty 2\pi r\, n(r) dr \int_0^\infty n(v_z) dv_z \left(v_z P_{\mathrm{hop}}(r, v_z)\right). \quad (2)$$

Here the same population distributions are used, but the spatial integration is over the central plane only, hence the $2\pi r$ Jacobean, and the hopping probability is multiplied by v_z to give a flux. We change to cylindrical coordinates to highlight our focus on the central plane. This flux integral gives the desired loss rate without any approximations about molecule orbits or plane-crossing frequency. This rigorous treatment provides precisely an overall scaling factor of π relative to the previous estimate.

The influence of this factor on the deconvolution procedure relates to the details of the two-body fitting routine. One plus two body fits $\dot{N} = -\gamma N - \beta N^2$ were performed to various decay trap curves, with the one body rate γ fixed to the value expected due to vacuum scattering and spin-flip loss. An example of such decay curves is shown in Fig. S1, where electric field is turned on suddenly after various hold times, which is motivated by the desire to vary the trapped sample density. With the stronger spin-flip loss, we also consider its effect beyond a pure one-body decay. Molecules whose orbits regularly intersect the loss region are lost, after which thermalization

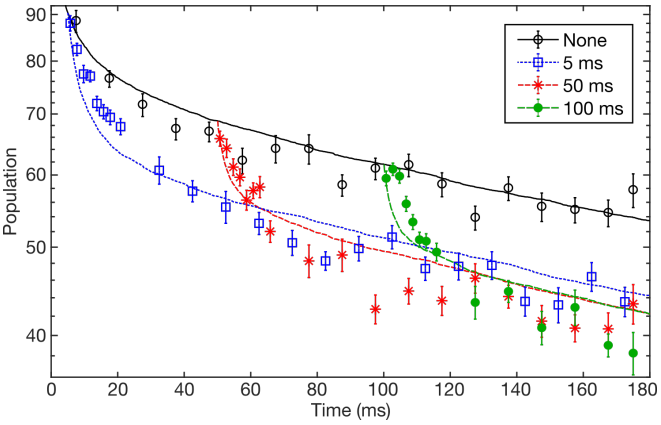

FIG. S1. Experimental data on electric field-induced loss with an attempted overlap to spin-flip loss simulations. The case of no electric field (black, solid, circles) is compared to electric fields of 3 kV/cm turned on after a wait time indicated in the legend.

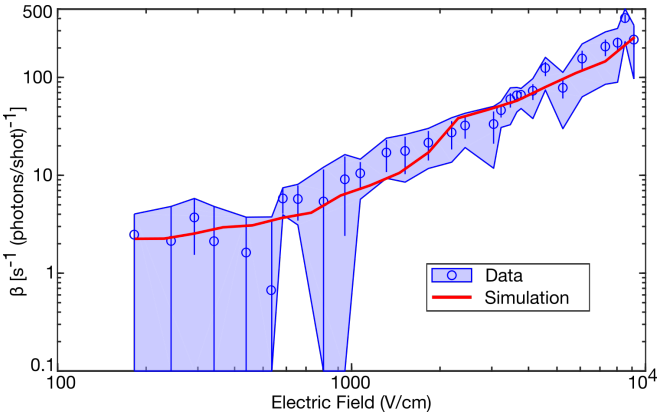

FIG. S2. Two body fits from [1] to experimental data like that in Fig. S1 but at various electric fields. The blue data points and shaded region are repeated from Fig. 3 of [1], where the shading indicates the variation that would be brought about by two-fold changes in γ from spin-flip losses. With a factor of three correction noted in this study, the spin flip loss simulation (thick red line) matches the original data within errorbars.

would be required to repopulate the loss prone trajectories of phase space. If thermalization is slow, spin-flip loss can have a rate that decreases over time, producing a time dependence of population like that of a two-body effect. Even though the possibility of a factor of two error in the calculated magnitude of spin-flip loss was considered in Ref. [1] (Repeated here in Fig. S2, shaded regions), the possibility of its influencing the data in a non-single-particle manner was not addressed. We note however that both the previous and current derivations of spin-flip loss assume a thermal distribution in the trap.

We have performed single particle Monte Carlo simulations of spin-flip loss to further investigate this effect, and we obtain curves such as shown with the experimental data in Fig. S1. We also performed the same one- plus two-body fitting procedure to the single particle spin-flip loss simulation traces, which yield two-body values that overlap with those derived in Ref. [1], see Fig. S2. This suggests that the spin-flip loss plays an important role in the observed loss data under applied electric fields, and the effect of inelastic collisions is marginal within the errorbars. Still, there are notable discrepancies if inelastic collis were not involved in the simulation, such as the disagreement between simulation and data in the initial rate of the decays in Fig. S1. One avenue to try and improve agreement would be to incorporate collisions in the simulation. There are many challenges in the quantitative application of these simulations, such as the existence of various partially trapped substates. The best path forward is to perform future collisional studies with the single-particle effect removed, as achieved in our most recent trap described in this paper [3].

B. Evaporation

Ref. [2] describes the processes of evaporation from a magnetic quadrupole trap and of depletion spectroscopy to measure the trap distribution. Both processes require two steps. First, molecules are transferred from the positive to the negative parity state by applying short pulses of microwaves tuned to a specific range of magnetic fields. After this transfer, the molecules are still trapped, and only by the subsequent application of a DC electric field to open avoided crossings can these opposite parity molecules escape from the trap. In the case of using depletion spectroscopy for thermometry, the microwave pulses tr ers only a small fraction of population between the opposite parity state to reflect the original population distribution [4]. A final step is necessary to measure the overall population in the trap by laser induced fluorescence. The crossings opened by electric field would only allow molecules in the upper 90% of the trap to escape, so it was assumed that a cold population insensitive to the spectroscopic technique would be building up in both parity states at low magnetic fields. Given the existence of spin-flip loss caused by the electric field at the center of the trap where such a cold population would build up, and given its strength for the relevant temperatures and electric fields (Tab. I of the main text [3]), the assumption of cold samples building up in the lower parity state must be reexamined.

Some of the temperature fits performed in Fig. 3 of Ref. [2] relied on this assumption, which we now no longer use. We rely on only the directly experimentally accessible spectra, such as those shown in panels (a-c) (Fig. 3 of Ref. [2]). After taking similar measurements repeatedly, the depletion spectra are found to be useful to identify enhancements in density caused by the evaporation. Figure S3 show such enhancements for evaporation sequences designed to achieve a twofold temperature reduction. The initial temperature of 59 ± 2 mK is higher than reported in Ref. [2], mostly due to an important correction to the molecular Hamiltonian recently discovered by inclusion of nearly one hundred ground and excited hyperfine levels [5].

Since depletion spectroscopy transfers only a fraction of molecules to the lower parity state at a specific magnetic field value, we integrate the total area enclosed by the spectroscopy curve, which is scaled according to the observed total population by laser induced fluorescence. This is necessary because depletion spectroscopy is performed with a train of short microwave pulses lasting over a total time of about a quarter of a trap oscillation, so that molecules are not at all frozen in place. Relative to a very brief spectroscopy pulse that would only deplete molecules in a given region at that particular instant, the use of a train of pulses over a longer period of time y us to sample molecules more widely to boost the signal

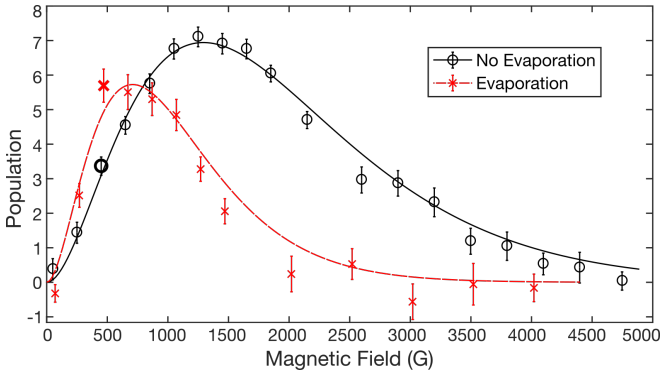

FIG. S3. Depletion spectroscopy spectra are obtained after evaporation (red x's) and without evaporation (black circles), with the integrated areas under the curves correspond to the total number of molecules detected. Solid lines are fits to Maxwell-Boltzmann distributions with temperatures of 59 ± 2 without evaporation (black), and 30 ± 3 for evaporation (red, dashed). The evaporation achieves a clear density enhancement in the vicinity of 500 G, where the line markers are bolded.

to noise ratio of spectroscopy. The spectroscopy gives a value that represents a small pr[illegible]tion of the true instantaneous population in a specific magnetic field region, but with a scaling factor that allows the signal to be constrained with the measured total number of molecules in the trap. We carefully include all of the steps in the error analysis leading to the error bars shown in Fig. S3.

Seeking another independent verification of the collisional effect, we have compared the populations under two closely related experimental sequences. The first is a normal evaporation sequence and the second is identical but with a time-reversed microwave frequency chirp, so that the population cut goes backwards from deep to shallow in the trap. This comparison subjects all molecules to the same integrated microwave power, and thus the two conditions should be equivalent in a situation with only single particle effects. With respect to collisional effects, the time-reversed case functions like a truncation, preventing molecules that would otherwise have collisionally thermalized to lower temperatures from doing so. To whatever extent an evaporation is successful in facilitating beneficial thermalizing collisions, the time-reversed condition should yield fewer molecules. We consistently observe this at the $(6 \pm 2)\%$ level, suggesting an evaporative effect despite the negative influence of spin-flip losses.

We have also developed the ability to reduce the size of the population without perturbing its phase space distribution, utilized in our new trap as described in the main text [3]. This ought to reduce the influence of collisional processes, but keep any single particle effects the same, thus disambiguating the two. Many possible approaches have key drawbacks, for example changing the partial pressure of water in our supersonic expansion would require changing the temperature of the valve and thereby influencing the initial speed of the beam. We opt for the application of microwaves during deceleration, leading to a probability for transitioning from a weak to strong field seeking state and being deflected out of the beam. We tune the microwaves to be resonant only at low magnitudes of electric fields, experienced by all molecules when flying through a de-energized stage just after switching. The microwaves are applied via microwave horn and have a long wavelength relative to the cloud, so that microwave power variations across the cloud are minimal. The microwaves are applied early during deceleration, so that the molecules have many stages of deceleration left to remix any outstanding asymmetries in the removal process. It is difficult to experimentally verify that the phase space distribution is truly unaffected, but in one projection of phase space, the time of flight profile of slowed molecules after deceleration, the distribution seems to be unaffected even by tenfold reductions using this technique.

While the role of collisional effects in Ref. [2] is reduced by spin-flip losses, especially at low temperatures below 10 mK, spectroscopic comparisons and evaporation subtractions do point to an evaporative effect. The development of forward to backward comparisons and homogeneous density reductions will allow us to further distinguish collisional effects from single particle dynamics in the next generation system.

C. Scaling Law Derivation

Here we derive the loss enhancement scaling law presented in Eqn. 3 of the main text [3], and repeated here:

$$\eta \propto \left(\frac{d_{\text{eff}} E}{\sqrt{\kappa \Delta}} \right)^{8/3}. \tag{3}$$

The key idea is to compare the surface areas of the loss regions with and without electric field. There is no exact loss region where a molecule is guaranteed to spin flip, but rather its velocity and direction contribute to the Landau-Zener probability (Eqn. 2, Ref. [3]). Nonetheless, for the purposes of a scaling law, we can assume the average thermal velocity v_T, and choose a probability threshold of $P > 1/e$. These assumptions allow us to define the loss region as the contour surface of energy κ where

$$\kappa = \sqrt{\hbar \dot{G}} = \sqrt{2 \hbar v_T B'}. \tag{4}$$

Here $\dot{G}$ is the rate of change in the energy gap between the trapped state and its spin flip partner, and B' is the magnetic field gradient along the strong axis of the trap.

We assume that the electric field is applied parallel to the strong axis of the quadrupole trap, which makes the loss plane, as defined by $\vec{E} \perp \vec{B}$, perpendicular to this

axis. This matches the geometry that has been realized in our experiment [1], and is the worst case, but by no more than a constant factor of $2\sqrt{2}$ relative to other directions the electric field could have.

Before application of electric field, the κ valued energy contour is the surface of an oblate ellipsoid of long radius $r_0 = 2\kappa/\mu_{\rm eff}B'$. Its area is then $2\pi \cdot 1.38\, r_0^2$, where the numeric factor relates to the specific $2:1$ aspect ratio of the ellipsoid and is hereafter neglected. When electric field is applied, the energy gap near the trap zero takes an unusual functional form. To derive it, we first assign spatial coordinates r and z denoting directions within and normal to the loss plane, respectively. Next we diagonalize the ground state hamiltonian of OH in mixed fields, see App. A of Ref. [4], or similarly for another species. Subtracting the energies of the trapped state and its spin-flip partner, and then series expanding the result yields:

$$G = \mu_{\rm eff}B'|z| + \alpha(\frac{1}{2}\mu_{\rm eff}B'r)^3 \frac{\Delta\sqrt{\beta\Delta^2 + d_{\rm eff}^2E^2}}{(d_{\rm eff}E)^4}, \quad (5)$$

plus higher order terms in r and z. The constants α and β are nearly unity for OH and will be ignored henceforth. The key feature, as discussed in the main text [3], is the cubic dependence G exhibits on r which leads to a much more severely oblate contours.

Now we can use Eqn. 5 to compute the surface area of the $G = \kappa$ contour. We specialize to the regime where $d_{\rm eff}E < \Delta$, so that $\Delta \approx \sqrt{\Delta^2 + d_{\rm eff}^2E^2}$. The radial extent of the surface can be solved by inverting $\kappa = G|_{z=0}$:

$$r_E = \frac{1}{\mu_{\rm eff}B'}\sqrt[3]{\frac{8\kappa(d_{\rm eff}E)^4}{\Delta^2}}. \quad (6)$$

The axial extent remains $z = \kappa/\mu_{\rm eff}B'$ for all $\vec{E}$. For large enough E, r_E dominates over this axial extent, so that the area is effectively $2\pi r_E^2$ and the loss area enhancement becomes $\eta = (r_E/r_0)^2$. Comparing the expressions for r_E and r_0, $\mu_{\rm eff}B'$ cancels and we have

$$\eta = \left(\frac{1}{2\kappa}\sqrt[3]{\frac{8\kappa(d_{\rm eff}E)^4}{\Delta^2}}\right)^2 = \left(\frac{d_{\rm eff}E}{\sqrt{\kappa\Delta}}\right)^{8/3}. \quad (7)$$

Now we address the domain of validity of this result. When E is small, Eqn. 5 only has a narrow range of validity, since the electric field only dominates in a very small region near the trap center. Outside, G retains a nearly linear dependence on r. This means that Eqn. 6 only holds for E above some threshold. For smaller E, r_E will simply not be significantly perturbed from its zero electric field value of $r_0 = 2\kappa/\mu_{\rm eff}B'$. The implication for the enhancement factor in Eqn. 7 is simply that it is only valid when it predicts an enhancement significantly greater than unity. In other words, Eqn. 7 holds when $d_{\rm eff}E > \sqrt{\kappa\Delta}$, but below this η gradually returns to unity. Eventually when $d_{\rm eff}E > \Delta$, the factor of $\sqrt{\beta\Delta^2 + d_{\rm eff}^2E^2}$ in Eqn. 5 is better approximated by $d_{\rm eff}E$, which leads to the modification $\eta \propto (d_{\rm eff}E)^2/\kappa^{4/3}\Delta^{2/3}$. Thus for these larger E-fields, the enhancement factor reduces in its dependence on electric field from order 8/3 to order 2. At this point, the loss is typically so large as to preclude all but the briefest trapping experiments, see Tab. I of the main text [3].

* Contributed equally. Email dave.reens@colorado.edu or hao.wu@colorado.edu.
† Present Address: 5. Physikalisches Institut and Center for Integrated Quantum Science and Technology (IQST), Universität Stuttgart, Pfaffenwaldring 57, 70569 Stuttgart, Germany

[1] B. K. Stuhl, M. Yeo, M. T. Hummon, and J. Ye, Molecular Physics **111**, 1798 (2013).
[2] B. K. Stuhl, M. T. Hummon, M. Yeo, G. Quéméner, J. L. Bohn, and J. Ye, Nature **492**, 396 (2012).
[3] See Main Text.
[4] B. K. Stuhl, M. Yeo, B. C. Sawyer, M. T. Hummon, and J. Ye, Physical Review A **85**, 033427 (2012).
[5] K. Maeda, M. L. Wall, and L. D. Carr, New Journal of Physics **17**, 45014 (2015).